Sonic hedgehog signaling is decoded by calcium spike activity in the developing spinal cord

Yesser H. Belgacem and Laura N. Borodinsky[1]

Department of Physiology and Membrane Biology and Institute for Pediatric Regenerative Medicine, Shriners Hospital for Children and University of California Davis School of Medicine, Sacramento, CA 95817

Edited* by Lynn T. Landmesser, Case Western Reserve University, Cleveland, OH, and approved February 9, 2011 (received for review December 5, 2010)

Evolutionarily conserved hedgehog proteins orchestrate the patterning of embryonic tissues, and dysfunctions in their signaling can lead to tumorigenesis. In vertebrates, Sonic hedgehog (Shh) is essential for nervous system development, but the mechanisms underlying its action remain unclear. Early electrical activity is another developmental cue important for proliferation, migration, and differentiation of neurons. Here we demonstrate the interplay between Shh signaling and Ca^{2+} dynamics in the developing spinal cord. Ca^{2+} imaging of embryonic spinal cells shows that Shh acutely increases Ca^{2+} spike activity through activation of the Shh coreceptor Smoothened (Smo) in neurons. Smo recruits a heterotrimeric GTP-binding protein-dependent pathway and engages both intracellular Ca^{2+} stores and Ca^{2+} influx. The dynamics of this signaling are manifested in synchronous Ca^{2+} spikes and inositol triphosphate transients apparent at the neuronal primary cilium. Interaction of Shh and electrical activity modulates neurotransmitter phenotype expression in spinal neurons. These results indicate that electrical activity and second-messenger signaling mediate Shh action in embryonic spinal neurons.

G protein | neuronal specification

Electrical activity is present in the developing nervous system before synapse formation. This activity, which is largely Ca^{2+} mediated, has an impact on several aspects of nervous system development. Neurotransmitter-mediated signaling regulates proliferation of cortical neuroblasts (1) and neuronal migration in the developing cerebellum (2), hippocampus (3), and subventricular zone (4). Motor neuron axons are guided by Ca^{2+}-mediated spontaneous patterned activity (5). The acquisition of neurotransmitter phenotype is regulated by Ca^{2+} spike activity in the developing brain (6, 7) and spinal cord (8, 9). In turn, all these activity-dependent events have a great impact on the establishment of connections among neurons and target cells (10, 11).

During early embryogenesis a gradient of Sonic hedgehog (Shh) establishes the dorsoventral patterning of the spinal cord (12–17). Shh persists after this process is finished and guides commissural spinal axons during midline crossing (18–22). In vertebrates, Shh binds to its receptor, Patched, allowing the recruitment and activation of Smoothened (Smo) in the primary cilium that triggers the regulation of targeted gene expression (23, 24). Smo is a seven-transmembrane receptor, and although its interaction with GTP-binding protein α-i (Gαi) has been demonstrated in vivo in *Drosophila* (25) and in vitro (25, 26), the functional relevance of this coupling in vertebrates has remained elusive (27–29). Activation of G protein-coupled receptors often engages second messengers such as Ca^{2+}, and cilia are structures especially suitable for coordinating second-messenger dynamics (30, 31). We investigated the interplay between electrical activity and Shh signaling in embryonic spinal neurons.

Results

Shh Signaling Acutely Regulates Levels of Ca^{2+} Spike Activity in the Developing Spinal Cord. Spontaneous Ca^{2+} spike activity spans 10 h of *Xenopus laevis* spinal cord development after neural tube closure (8, 32). We imaged cells of the ventral and dorsal surfaces of the developing neural tube and found that spiking cells are embryonic neurons (283 of 290 spiking cells expressed the neuronal marker *N*-β-tubulin). On the other hand, neural progenitors, identified by sex-determining region Y-box 2 (Sox2) expression, do not exhibit Ca^{2+} spikes (none of 148 $Sox2^{+}$ cells spiked) (Fig. 1). Both the incidence of spiking cells and the frequency of Ca^{2+} spikes are higher in ventral cells than in their dorsal counterparts (Fig. 2 *A–C*), demonstrating a ventral-to-dorsal gradient that parallels the Shh gradient (12–14, 16) in the embryonic spinal cord. To probe this correspondence, we first confirmed the presence of Shh and its coreceptor Smo in the developing spinal cord (Fig. S1 *A* and *B*) and then investigated the influence of modulators of Shh signaling on Ca^{2+} spike activity. We imaged Ca^{2+} dynamics in cells of the ventral surface of the *Xenopus* spinal cord and found that recombinant N-terminal Shh peptide (*N*-Shh) acutely increases Ca^{2+} spike activity in a dose-dependent manner (Fig. 2 *D–F*). This effect is mimicked by an agonist for Smo (SAG) and is prevented by cyclopamine, a Smo antagonist (Fig. 2*G*). Moreover, overexpression of SmoM2, a constitutively active form of Smo (33), in developing embryos after neural tube closure increases Ca^{2+} spike activity (Fig. 2 *H–K* and Fig. S1*C*).

To determine whether an endogenous gradient of Shh is able to imprint a gradient of Ca^{2+} spike activity on neurons positioned across it, we first cultured embryonic spinal cells and demonstrated that the effects of exogenous Shh and cyclopamine on Ca^{2+} spike activity observed in vivo also are evident in vitro (Fig. S2). We then designed an in vitro system of neuron/notochord explant coculture and found that the incidence of spiking cells is higher in the half of the field containing the explant than in the other half (Fig. 2*L*). This differential distribution of spiking cells is prevented by the addition of cyclopamine, suggesting that Shh secreted from the notochord explant is responsible for the increased Ca^{2+} spike activity.

These results identify a signaling pathway for Shh involving the activation of its canonical coreceptor Smo that, in turn, induces an increase in Ca^{2+} spike activity in developing spinal neurons. This dose-dependent effect suggests that Ca^{2+} spike activity may serve as a readout of the Shh gradient.

To elucidate further the molecular mechanisms underlying Shh-induced increase in Ca^{2+} spike activity, we investigated the participation of Ca^{2+} influx and Ca^{2+} release from intracellular stores, both required for the generation of Ca^{2+} spikes (34). Shh fails to increase Ca^{2+} spike activity when voltage-gated Ca^{2+} channels are blocked or extracellular Ca^{2+} is removed, indicating that Shh-induced Ca^{2+} spikes depend on extracellular Ca^{2+} entry (Fig. 3*A*). Smo is a seven-pass transmembrane protein capable of

Author contributions: Y.H.B. and L.N.B. designed research; Y.H.B. performed research; Y.H.B. and L.N.B. analyzed data; and Y.H.B. and L.N.B. wrote the paper.

The authors declare no conflict of interest.

*This Direct Submission article had a prearranged editor.

Freely available online through the PNAS open access option.

[1]To whom correspondence should be addressed. E-mail: lnborodinsky@ucdavis.edu.

This article contains supporting information online at www.pnas.org/lookup/suppl/doi:10.1073/pnas.1018217108/-/DCSupplemental.

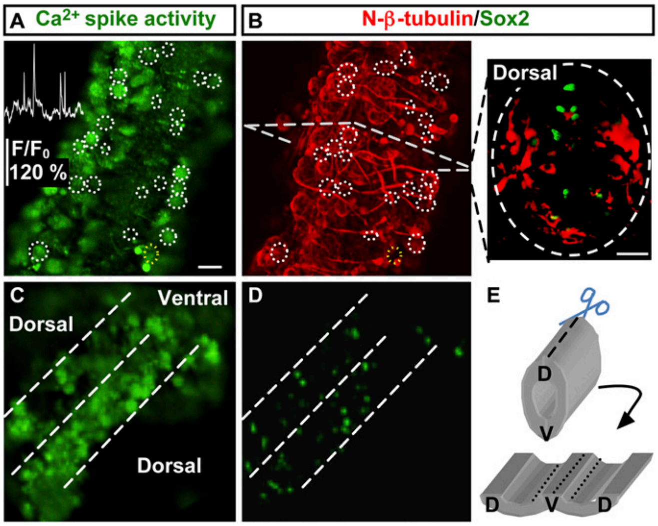

Fig. 1. Spiking cells in the developing neural tube are postmitotic neurons. (*A*) Ca^{2+} imaging of the ventral spinal cord of a stage-24 (26-h-postfertilization) embryo for 20 min. Circles identify cells spiking during 20-min recording. *Inset* shows Ca^{2+} spike activity for the cell outlined in yellow. (*B*) (*Left*) After imaging, the same preparation was whole-mount immunostained for Sox2 and *N*-β-tubulin. (*Right*) Immunostaining of a transverse section of the spinal cord from a stage-24 embryo. (*C*) Ca^{2+} imaging of an open-book spinal cord preparation. (*D*) Whole-mount immunostaining of the same preparation for Sox2 and *N*-β-tubulin. (*E*) Diagram of the open-book spinal cord preparation shown in *C* and *D*. D, dorsal; V, ventral. (Scale bars, 20 μm.)

recruiting heterotrimeric Gαiβγ protein (25, 26). Gαi activation inhibits adenylate cyclase, decreasing cAMP levels and hence inhibiting protein kinase A (PKA). The presence of pertussis toxin (PTX) or overexpression of a constitutively active form of PKA (a mutated catalytic subunit, C_{QR}) (35) immediately following neural tube closure blocks the Shh-induced increase in Ca^{2+} spike activity (Fig. 3*B* and Fig. S3). In contrast, Shh increases Ca^{2+} spike activity following overexpression of a dominant negative form of PKA (a mutated regulatory subunit, R_{AB}) (Fig. 3*B* and Fig. S3) (36), indicating that the Shh-induced effect depends on PTX-sensitive Gαβγ protein and subsequent PKA inhibition.

Recruitment of G protein also can activate phospholipase C (PLC) that in turn increases inositol triphosphate (IP3) levels and induces Ca^{2+} release from internal stores. Pharmacological blockade of either PLC or IP3 receptors (IP3R) prevents Shh-induced Ca^{2+} spike activity, suggesting that Ca^{2+} stores are required for the Shh-mediated effect (Fig. 3*C*). In turn, emptying of Ca^{2+} stores has been proposed as a trigger for transient receptor potential cation channel (TRPC) activation leading to Ca^{2+} influx (37). *Xenopus* TRPC1 (*x*TRPC1) has been cloned (38) and is expressed in embryonic spinal neurons (39, 40). Pharmacological inhibition of TRPCs or molecular knockdown of *x*TRPC1 (Fig. S4) blocks the Shh-induced increase in Ca^{2+} spike activity (Fig. 3*D*). These results identify second messengers and channels involved in Shh signaling in embryonic spinal neurons.

Shh Signaling Induces Synchronous Ca^{2+} Spikes and IP3 Transients at the Neuronal Primary Cilium. In vertebrates the Shh signaling machinery clusters and functions in primary cilia (Fig. S1*B*, *Inset*) (23, 24). We find that IP3R localize at the base of the neuronal primary cilium (Fig. 4*A*), whereas Gαi and TRPC1 are distributed along its tip and shaft, respectively (Fig. 4 *B* and *C*). Incubation of neuronal cultures with SAG expands Gαi localization to the full extent of the cilium (Fig. 4*D*), resembling the change in Smo distribution in NIH 3T3 cells after stimulation with Shh (23, 24). To assess the interplay between Shh and Ca^{2+} spike activity dynamically, we microinjected mRNA encoding an RFP-tagged pleckstrin homology (PH) domain from phospholipase C-δ1 [mRFP-PH(PLCδ)], a molecular probe for IP3 levels (41), in developing embryos to visualize simultaneously Shh-induced Ca^{2+} spikes and IP3 transients. When Smo is overexpressed (Fig. S1*C*) and in the presence of SAG, we observed localized IP3 transients at the primary cilium synchronized with Ca^{2+} spikes (Fig. 4 *E*–*H*). The onset of IP3 transients precedes the onset of Ca^{2+} spikes by 8 ± 2 s (mean ± SEM; $n = 17$) (Fig. 4*H*), suggesting that Shh-induced Ca^{2+} spikes depend on IP3-induced Ca^{2+} release from intracellular stores. The incidence of synchronized Ca^{2+} spikes and IP3 transients is highest in the presence of SAG and is abolished by cyclopamine (Fig. S5). The restricted visualization of Shh-induced IP3 transients at the primary cilium probably is caused by localized signaling (23) and not by the inability of the probe to reveal cytosolic changes in IP3. Indeed, this bioprobe is able to report global increases in IP3 levels elicited by dihydroxyphenylglycol (DHPG), a metabotropic glutamate receptor (mGluR) agonist (Fig. S6). These results suggest that Shh signaling is able to elicit fast and localized responses at the primary cilium by recruiting second messengers.

Regulation of Neurotransmitter Specification by Shh Signaling Relies on the Interplay with Ca^{2+} Spike Activity. Neurotransmitter specification is a crucial event of neuronal differentiation that enables the establishment of functional circuits in the developing nervous system. Ca^{2+} spike activity modulates expression of neurotransmitter phenotype in developing neurons, and activity-dependent components that participate in the transcriptional regulation of the GABAergic phenotype have been identified recently (9). Therefore, we investigated whether Shh signaling acts on electrical activity to modulate GABAergic phenotype specification (Fig. S7*A*). We find that enhancement or inhibition of Shh signaling mimics the effect on GABAergic phenotype expression observed when Ca^{2+} spike activity is enhanced or suppressed, respectively (Fig. 5*A*). The numbers of spinal cells or ventral progenitors do not change in manipulated embryos (Fig. S7*B*), in agreement with the constancy in domains of specified ventral progenitors observed in chicken embryos in which Shh signaling had been perturbed at late developmental stages (42). Imposition of changes in Ca^{2+} spike activity (Fig. S8) occludes SAG- or cyclopamine-induced phenotypes (Fig. 5*A*). These results suggest that Shh signals to engage Ca^{2+} spike activity in the process of neurotransmitter specification revealing a function of Shh in postmitotic neuron differentiation.

Discussion

We propose a model (Fig. 5*B*) in which Shh activates Smo at the primary cilium, resulting in the recruitment of PTX-sensitive Gαβγ protein that leads to activation of PLC and increases in IP3 levels. Opening of IP3R-operated stores and activation of TRPC1 and voltage-gated channels result in an increase of Ca^{2+} spike activity. Activated Smo also inhibits PKA, which can inhibit IP3-induced Ca^{2+} release (43). Hence, modulation of Ca^{2+} spike activity may occur by pathways that are parallel or convergent to the one operated by PLC. The precise sequence in which Ca^{2+} influx and stores operate for the generation of Shh-induced Ca^{2+} spikes remains to be addressed. For instance, activation of TRPC1 by emptiness of Ca^{2+} stores may depolarize the membrane, leading to the activation of voltage-gated channels. The effect on spinal neuron differentiation of this signal transduction pathway, connecting Shh with Ca^{2+} spike activity, demonstrates integration of genetically driven and electrical activity-dependent mechanisms. This interplay allows greater plasticity and more efficient proofreading of nervous system development (44).

Shh drives the dorsoventral patterning of the neural tube early in development by regulating gene expression. Dorsoventral

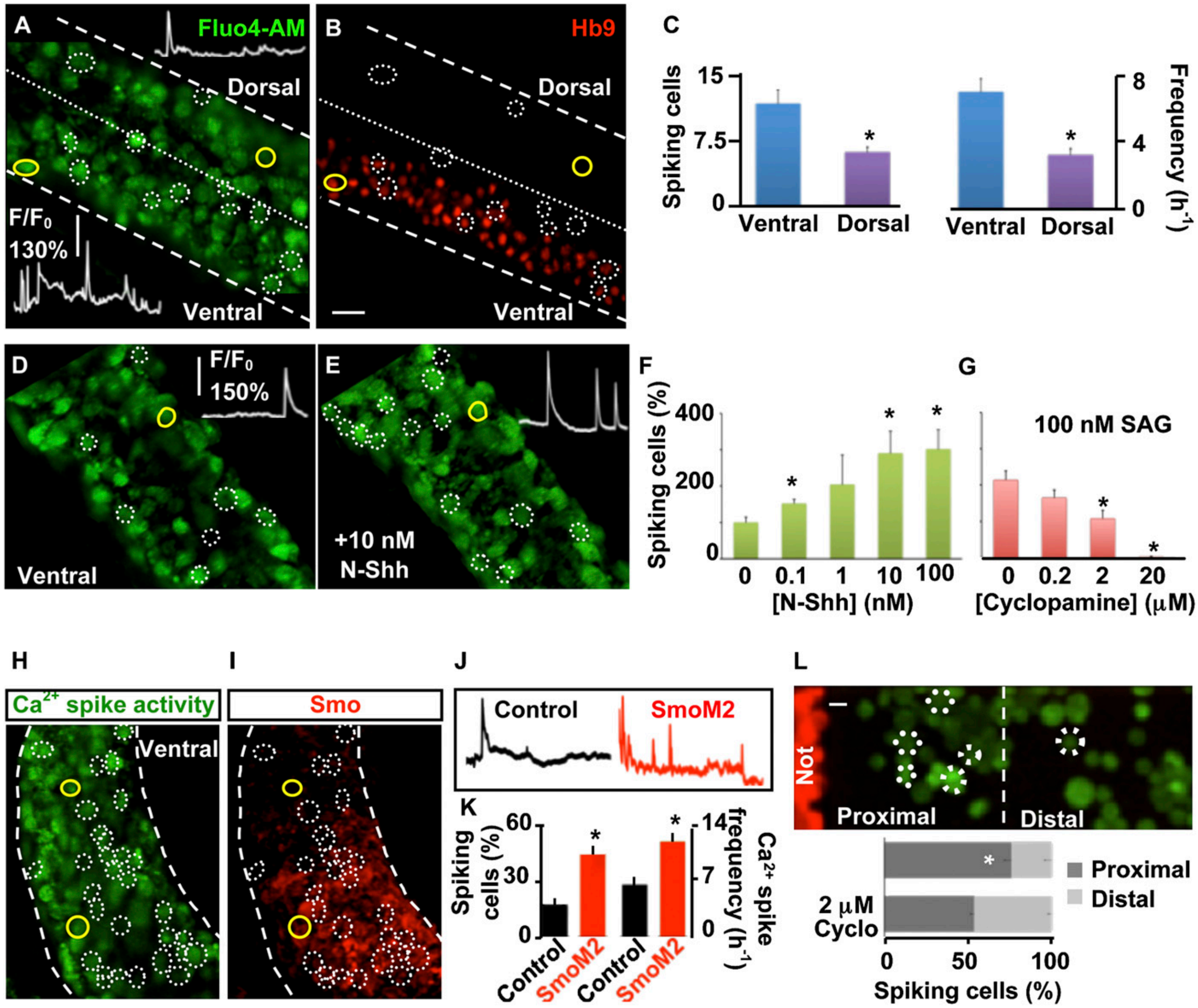

Fig. 2. Shh increases Ca^{2+} spike activity of developing spinal neurons. (*A*) Lateral view of a developing spinal cord showing higher levels of Ca^{2+} spike activity in the ventral than in the dorsal neural tube (stage 24). (*B*) After imaging, the same preparation was whole-mount immunostained for homeodomain protein Hb9, a ventrally expressed neuronal marker, to indicate its dorsoventral orientation. Circles identify cells spiking during 20-min recording, and *Insets* in *A* show Ca^{2+} spike activity for cells outlined in yellow. (*C*) Incidence of spiking cells per neural tube and frequency of Ca^{2+} spikes in ventral and dorsal spinal neurons. (*D* and *E*) Ventral view of stage-24 developing spinal cord in the absence (*D*) or presence (*E*) of *N*-Shh. *Insets* show Ca^{2+} spike activity during 15-min recording from the same cell (outlined in yellow). (*F*) Dose–response curve for *N*-Shh–induced Ca^{2+} spike activity. Data are mean ± SEM percent of spiking cells in the presence of N-Shh compared to number of cells spiking before addition of N-Shh (0). (*G*) Dose–response curve for cyclopamine blockade of Ca^{2+} spike activity induced by SAG. Data are mean ± SEM percent of spiking cells in the presence of SAG and cyclopamine compared to number of cells spiking before addition of cyclopamine (0). (*H*–*K*) Expression of SmoM2 increases Ca^{2+} spike activity. (*H*) Electroporation of a stage-19 embryo with SmoM2 demonstrates a higher incidence of Ca^{2+} spike activity 6 h after electroporation (stage 24) in electroporated cells (red) than in nonelectroporated cells (black). (*I*) Effective overexpression of SmoM2 was verified by whole-mount immunostaining against Smo after Ca^{2+} imaging. Circles identify cells spiking during recording. (*J*) Ca^{2+} spike activity during 20-min recording for immunonegative and immunopositive cells outlined in yellow in *H* and *I*. (*K*) Bar graphs show mean ± SEM percent incidence of spiking cells and spike frequency for electroporated (SmoM2) and nonelectroporated (Control) cells. *n* = 5 stage-24 (26-h postfertilization) embryos per experimental group (*C*–*K*). (*L*) Endogenous Shh released by the notochord increases Ca^{2+} spike activity of neurons. (*Upper*) Dissociated neuron/notochord explant (Not) coculture. (*Lower*) The imaged field was divided in halves proximal and distal to the notochord explant. Values are mean ± SEM percent of spiking cells in proximal and distal regions in the absence or presence of cyclopamine (Cyclo). *n* = 5 independent cultures; *$P < 0.05$. (Scale bars, 20 μm.)

excitability of the developing spinal cord may be set by this transcription-dependent mechanism. Later in development Shh may contribute to maintaining and modulating the dorsoventral gradient of electrical activity in spinal neurons independently of transcription, as suggested in the present study. Specific patterns of electrical excitability along the dorsoventral axis of the developing spinal cord have been identified in several species. In *Xenopus* embryos, dorsal spinal cells comprising Rohon–Beard sensory neurons and a minority of interneurons generate sparse numbers of action potentials upon sustained depolarization; in contrast, ventral cells, including motor neurons and the majority of interneurons, fire repetitively (45). Similarly, in larval zebrafish, recruitment of excitatory dorsal spinal neurons requires higher levels of stimulation than do their ventral counterparts, whereas inhibitory spinal neurons show the opposite pattern; this topography underlies distinctive swimming behaviors (46). This

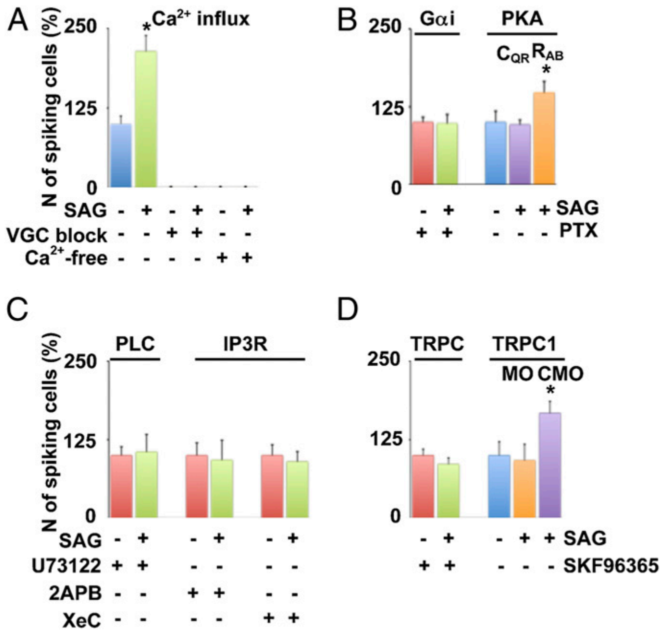

Fig. 3. Molecular identification of the components linking Shh and Ca^{2+} spike activity. (*A–D*) Ca^{2+} imaging of the ventral spinal cord. (*A*) Ca^{2+} influx was blocked by a mixture of Na^+ and Ca^{2+} voltage-gated channel blockers (VGC block) or by perfusion with a Ca^{2+}-free medium (Ca^{2+}-free). (*B*) Gαi was inhibited by 10 mM PTX. Perturbations of PKA activity were implemented by electroporating constitutively active (C_{QR}) or dominant negative (R_{AB}) forms of PKA in stage-19 embryos. Ca^{2+} imaging was performed 6 h after electroporation. (*C*) PLC was inhibited by 10 μM U73122, and IP3R were inhibited by 20 μM 2-aminoethoxydiphenyl borate (2-APB) or 20 μM xestospongin C (XeC). (*D*) TRPC channels were blocked by 50 μM SKF96365 or by molecular knockdown with *x*TRPC1 morpholino (MO). Control morpholino (CMO). Values are mean ± SEM percent incidence of spiking cells in the ventral surface of neural tubes compared with control (30-min recording before addition of 100 nM SAG). n = 5 stage-24 (26-h postfertilization) embryos per experimental group; $*P < 0.05$ (*A–D*).

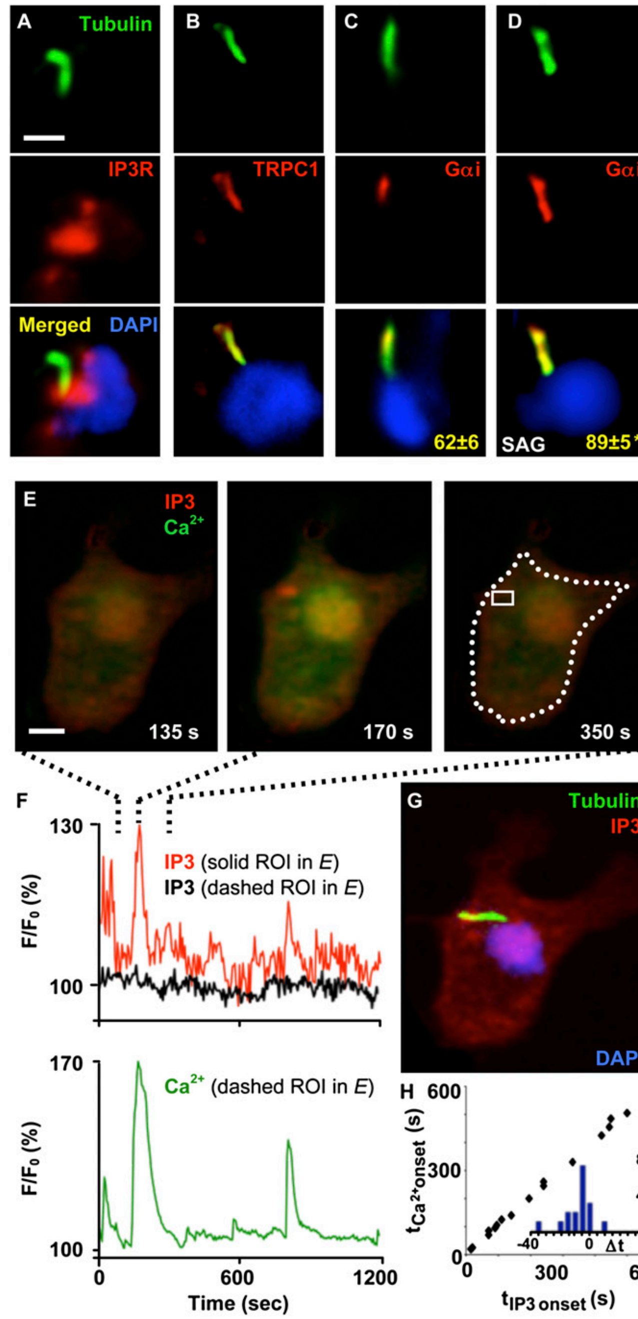

Fig. 4. Shh and second-messenger signaling converge at the neuronal primary cilium. (*A–D*) Immunostaining of immature spinal neurons grown in vitro for 7 h. Acetylated tubulin staining is shown in green, and DAPI staining is shown in blue. (*A*) IP3R (red) localize at the base of the primary cilium. (*B*) TRPC1 (red) localizes to the primary cilium. (*C* and *D*) Gαi protein (red) localization at the primary cilium expands when Shh signaling is enhanced. Numbers correspond to the mean ± SEM percent of acetylated tubulin labeling that overlaps with Gαi staining at the primary cilium in the absence (*C*) or presence (*D*) of 100 nM SAG for 4 h. n = 10 cells per condition; $*P < 0.005$. (*E* and *F*) Simultaneous Ca^{2+} and IP3 imaging reveals synchronous transients. (*E*) Images correspond to a time before (*Left*), during (*Center*), and after (*Right*) the spike indicated in the trace in *F*. (*F*) Traces represent the changes in fluorescence intensity for IP3 and Ca^{2+} probes in regions of interest (ROI) indicated in *E*, *Right*. (*G*) IP3 transients are apparent at the primary cilium. The cell is the same shown in *E*, stained with DAPI (blue) and anti-acetylated tubulin (green) and overlapped with IP3 frame (red) corresponding to the peak of the transient shown in *E*, *Center*. (Scale bars, 10 μm.) (*H*) Synchronicity of Ca^{2+} and IP3 transients. Graph represents onset time of Ca^{2+} spikes vs. onset time of IP3 transients during simultaneous recordings. *Inset* represents the histogram of the difference between onset times; $\Delta t = tIP3 - tCa^{2+}$.

profile appears to be rooted in early development through an orderly addition of neurons to the developing network (47). In chicken embryos, neuronal activity is higher in the ventral two thirds of the spinal cord than in the dorsal region (48). Taken together these studies suggest that the patterning of excitability along the dorsoventral axis of the developing spinal cord is highly conserved and relevant for proper spinal cord development.

The necessity of a subcellular compartment such as the primary cilium for Shh signaling (12, 23, 24, 49, 50) allows the spatiotemporal integration of two second-messenger codes generated by Ca^{2+} and IP3 transients. The universal character of second-messenger signaling predicts that this pathway is common to different cell types, although different classes of cells may exhibit distinctive second-messenger dynamics (51, 52). It will be of interest to investigate how these steps of decoding Shh signaling are connected to other elements of its canonical pathway and to determine the mechanisms by which the interactions between Shh, IP3, and Ca^{2+} are interpreted and translated into expression of specific genes.

Materials and Methods

Cell Cultures. Cell cultures were grown as previously described (8). For neuron–notochord explant cocultures, neuron-enriched cultures from stage-17 embryos were prepared as previously described (8), grown for 5 h, and loaded with 1 μM fluo4-AM (Invitrogen). A 0.004-mm^3 piece of notochord from a stage-24 embryo previously microinjected at the two-cell stage with dextran-Alexa Fluor 594 conjugate (Invitrogen) was placed in the neuronal culture.

Ca^{2+} Imaging. Ca^{2+} imaging was performed as described previously (8). Stage-23 to -26 (24.75- to 29.5-h-old) neural tubes were exposed and loaded with 1

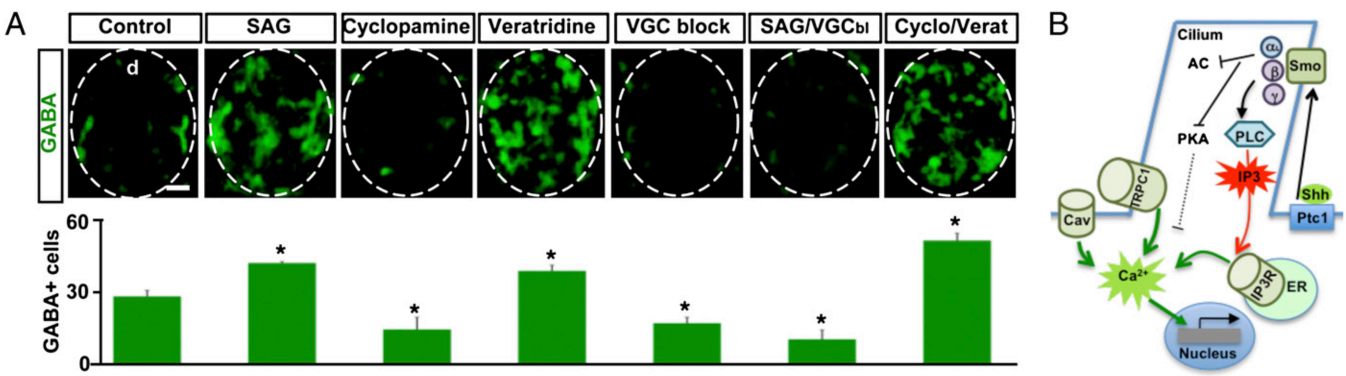

Fig. 5. Ca^{2+} spike activity is necessary for Shh-induced spinal neuron differentiation. (*A*) (*Upper*) Immunostaining of transverse sections of the spinal cord from embryos treated with agents indicated in the figure. Cyclo, cyclopamine; d, dorsal; Verat, veratridine; VGC block and VGC_{bl}, voltage-gated Na^+ and Ca^{2+} channel blockers. (*Lower*) Graph shows mean ± SEM GABA-immunopositive cells/100 μm of spinal cord. $n \geq 5$ stage-34 (45-h postfertilization) embryos per experimental group; $*P < 0.05$. (Scale bar, 20 μm.) (*B*) Model of the molecular mechanisms underlying Shh-induced Ca^{2+} spikes. α, β, γ, subunits of the heterotrimeric G protein; AC, adenylate cyclase; Cav, voltage-gated Ca^{2+} channels; ER, endoplasmic reticulum; Ptc1, Patched1. Details are given in *Discussion*.

μM fluo4-AM. Ca^{2+} imaging was performed at an acquisition rate of 0.2 Hz with a Nikon Swept-field confocal microscope. The effects of proteins and drugs were assessed by recording for 30 min before and after addition of each agent. Changes in Ca^{2+} spike activity were assessed by comparisons of the two recordings (paired *t* test).

Drugs were incubated for 30 min with the exception of pertussis toxin (PTX) (Tocris) for 1 h and N-terminal Sonic hedgehog (Shh) peptide (*N*-Shh) (R&D Systems) and Shh agonist (SAG) (Calbiochem) for 10 min. The concentrations of drugs used were *N*-Shh: 0.1–100 nM; cyclopamine: 0.2–10 μM (LC Laboratories), SAG: 100 nM; Na^+ and Ca^{2+} voltage-gated channel blockers (VGC block): 20 nM calcicludine (Calbiochem), 1 μM GVIA ω-conotoxin, 1 μM flunarizine, and 1 μg/mL tetrodotoxin (Sigma); voltage-gated Na^+ channel agonist: 1 μM veratridine (Sigma); GTP-binding protein alpha-i (Gαi) inhibitor: 10 mM PTX; phospholipase C (PLC) inhibitor: 10 μM U73122 (Tocris); inositol triphosphate 3 (IP3) receptor (IP3R) inhibitors: 20 μM 2-aminoethoxydiphenyl borate (2-APB) (Tocris) and 20 μM Xestospongin C (XeC) (Calbiochem); and transient receptor potential cation channel (TRPC) inhibitor: 50 μM SKF96365 (Tocris).

IP3 Imaging. RFP-PH(PLCδ), an RFP-tagged pleckstrin homology (PH) domain from phospholipase C–δ1 serving as a $PI(4,5)P_2/IP_3$ biosensor, was used to monitor IP3 levels in cultured cells (41). RFP-PH(PLCδ) was subcloned in the $pCS2^+$. The RFP-PH(PLCδ) sequence was amplified by PCR. A BamH1 restriction site was added to the sense primer (sense: AGTTACAGGATCC-GCTGGTTTAGTGAACCGTCAG; antisense: AAAACCTCTACAAATGTGGTATGG-CTGATT). PCR product and plasmid were then digested by BamH1 and EcoR1. After ligation and purification, mRNA was synthesized as previously described (8). Neuron-enriched cultures prepared from neural plates of embryos microinjected at the two-cell stage with 700 pg of mRNA encoding RFP-PH(PLCδ) and 300 pg of human Smoothened (Smo) were incubated for 10 min with 100 nM SAG and confocally imaged at 0.2 Hz for 20 min.

In Vivo Gene Misexpression. For SmoM2 overexpression, mRNAs were synthesized as previously described (8). Four nanoliters of 400 ng/μL mRNA encoding SmoM2 along with 20 mg/mL Alexa Fluor 594 dextran were microinjected in the neural tube lumen of stage-19 embryos (20.75 h postfertilization) followed by electroporation (10 pulses of 70 V and 90-ms duration). For protein kinase A (PKA) misexpression, PCR products containing the T7 RNA polymerase promoter were used to synthesize mRNAs encoding a dominant negative form (R_{AB}) or a constitutively active (C_{QR}) form of PKA. The primers used were sense, TAATACGACTCACTATAGGGACTC-CGTAGCTCCAGCTTCAC and antisense, GTGAAACCCCGTCTCTACCA. Four nanoliters of 250 ng/μL mRNA encoding either of these two constructs along with 20 mg/mL Alexa Fluor 594 dextran were microinjected in the neural tube lumen of stage-19 embryos followed by electroporation (10 pulses of 70 V and 90-ms duration). Controls were electroporated with Alexa Fluor 594 dextran only. For *Xenopus* TRPC (*x*TRPC1) knockdown, embryos at the two-cell stage were microinjected with 100 pg *x*TRPC1 morpholino or 5-mispaired control morpholino (MO and CMO, respectively; Genetools) along with 20 mg/mL Alexa Fluor 594 dextran. Morpholino oligonucleotides were designed as in Wang and Poo, 2005 (40). For Smo overexpression, mRNA was synthesized as previously described (8). Three hundred picograms mRNA encoding human Smo were microinjected bilaterally in both blastomeres of embryos at the two-cell stage.

Western Blots. Western blots were performed as previously described (10). Protein extracts were obtained from 10 dissected neural tubes from stage-25 embryos for each experimental group using the following antibodies: anti-Smo, 1:1,000 (Sigma); anti-GAPDH, 1:1,000, anti-PKAIα reg, 1:100, and anti-PKAα cat, 1:100 (Santa Cruz Biotechnology); and anti-TRPC1, 1:300, Osense and gift from G. J. Barritt (Flinders University, Adelaide, Australia). Secondary peroxidase-conjugated antibodies (Jackson ImmunoResearch) were used at 1:5,000 dilution.

In Vivo Drug Delivery. In vivo drug delivery was performed as previously described (8, 10). Agarose beads (80 μm; BioRad) were loaded for at least 1 h with 1 mM veratridine and the Ca^{2+} spike blockers 200 nM calcicludine, 10 μM GVIA ω-conotoxin, 10 μM flunarizine, 10 μg/mL tetrodotoxin, 1 μM SAG, and 200 μM cyclopamine, or a combination of these agents and implanted in stage-19 embryos (20-h postfertilization). Stage-34 (2-d postfertilization) larvae were sectioned for immunostaining.

Immunostaining. Samples were fixed with 4% paraformaldehyde (PFA) and processed for immunostaining as previously described (8). Incubations with primary and secondary antibodies were carried out overnight at 4 °C and for 2 h at 23 °C, respectively. Primary antibodies used were directed to acetylated tubulin, 1:1,000 (Sigma); GαI, 1:50, and IP3R 1:50, (Santa Cruz Biotechnology); TRPC1, 1:50 (Developmental Studies Hybridoma Bank); sex-determining region Y-box 2 (Sox2), 1:50 (R&D Systems); GABA, 1:100 (Millipore); *N*-tubulin, 1:1,000 (Sigma); Shh, 1:100 (Developmental Studies Hybridoma Bank); Smo, used for detecting endogenous Smo, 1:20 (Abcam); Smo, used for detecting overexpressed human Smo, does not recognize endogenous Smo 1:300 (Sigma). Immunoreactive cells were counted in at least 20 consecutive 12-μm sections per embryo.

Data Collection and Statistics. Regions of interest for detection of IP3 levels at the primary cilium were defined by the area labeled by anti-acetylated tubulin, a marker of primary cilium.

At least five samples were analyzed for each group from at least three independent clutches of embryos. Statistical tests used were paired or unpaired *t* test or ANOVA when multiple experimental groups were compared simultaneously; $P < 0.05$.

ACKNOWLEDGMENTS. We thank N. C. Spitzer for critical comments on the manuscript. We thank F. De Sauvage for the Smo and SmoM2 construct, G. S. McKnight for PKA constructs, G. J. Barritt for the *x*TRPC1 antibody, and T. Meyer for the RFP-PH(PLCδ) construct. This work was supported by an award to L.N.B. from The Esther A. and Joseph Klingenstein Fund, a grant to L.N.B. from The Shriners Hospital for Children, and a postdoctoral fellowship to Y.H.B. from The Shriners Hospital for Children.

1. LoTurco JJ, Owens DF, Heath MJ, Davis MB, Kriegstein AR (1995) GABA and glutamate depolarize cortical progenitor cells and inhibit DNA synthesis. *Neuron* 15:1287–1298.
2. Komuro H, Rakic P (1996) Intracellular Ca2+ fluctuations modulate the rate of neuronal migration. *Neuron* 17:275–285.
3. Manent JB, et al. (2005) A noncanonical release of GABA and glutamate modulates neuronal migration. *J Neurosci* 25:4755–4765.
4. Bolteus AJ, Bordey A (2004) GABA release and uptake regulate neuronal precursor migration in the postnatal subventricular zone. *J Neurosci* 24:7623–7631.
5. Hanson MG, Landmesser LT (2004) Normal patterns of spontaneous activity are required for correct motor axon guidance and the expression of specific guidance molecules. *Neuron* 43:687–701.
6. Demarque M, Spitzer NC (2010) Activity-dependent expression of Lmx1b regulates specification of serotonergic neurons modulating swimming behavior. *Neuron* 67: 321–334.
7. Dulcis D, Spitzer NC (2008) Illumination controls differentiation of dopamine neurons regulating behaviour. *Nature* 456:195–201.
8. Borodinsky LN, et al. (2004) Activity-dependent homeostatic specification of transmitter expression in embryonic neurons. *Nature* 429:523–530.
9. Marek KW, Kurtz LM, Spitzer NC (2010) cJun integrates calcium activity and tlx3 expression to regulate neurotransmitter specification. *Nat Neurosci* 13:944–950.
10. Borodinsky LN, Spitzer NC (2007) Activity-dependent neurotransmitter-receptor matching at the neuromuscular junction. *Proc Natl Acad Sci USA* 104:335–340.
11. Catalano SM, Shatz CJ (1998) Activity-dependent cortical target selection by thalamic axons. *Science* 281:559–562.
12. Chamberlain CE, Jeong J, Guo C, Allen BL, McMahon AP (2008) Notochord-derived Shh concentrates in close association with the apically positioned basal body in neural target cells and forms a dynamic gradient during neural patterning. *Development* 135:1097–1106.
13. Chen MH, Li YJ, Kawakami T, Xu SM, Chuang PT (2004) Palmitoylation is required for the production of a soluble multimeric Hedgehog protein complex and long-range signaling in vertebrates. *Genes Dev* 18:641–659.
14. Echelard Y, et al. (1993) Sonic hedgehog, a member of a family of putative signaling molecules, is implicated in the regulation of CNS polarity. *Cell* 75:1417–1430.
15. Ericson J, Morton S, Kawakami A, Roelink H, Jessell TM (1996) Two critical periods of Sonic Hedgehog signaling required for the specification of motor neuron identity. *Cell* 87:661–673.
16. Lum L, Beachy PA (2004) The Hedgehog response network: Sensors, switches, and routers. *Science* 304:1755–1759.
17. Roelink H, et al. (1995) Floor plate and motor neuron induction by different concentrations of the amino-terminal cleavage product of sonic hedgehog autoproteolysis. *Cell* 81:445–455.
18. Bourikas D, et al. (2005) Sonic hedgehog guides commissural axons along the longitudinal axis of the spinal cord. *Nat Neurosci* 8:297–304.
19. Charron F, Stein E, Jeong J, McMahon AP, Tessier-Lavigne M (2003) The morphogen sonic hedgehog is an axonal chemoattractant that collaborates with netrin-1 in midline axon guidance. *Cell* 113:11–23.
20. Okada A, et al. (2006) Boc is a receptor for sonic hedgehog in the guidance of commissural axons. *Nature* 444:369–373.
21. Parra LM, Zou Y (2010) Sonic hedgehog induces response of commissural axons to Semaphorin repulsion during midline crossing. *Nat Neurosci* 13:29–35.
22. Yam PT, Langlois SD, Morin S, Charron F (2009) Sonic hedgehog guides axons through a noncanonical, Src-family-kinase-dependent signaling pathway. *Neuron* 62:349–362.
23. Corbit KC, et al. (2005) Vertebrate Smoothened functions at the primary cilium. *Nature* 437:1018–1021.
24. Rohatgi R, Milenkovic L, Scott MP (2007) Patched1 regulates hedgehog signaling at the primary cilium. *Science* 317:372–376.
25. Ogden SK, et al. (2008) G protein Galphai functions immediately downstream of Smoothened in Hedgehog signalling. *Nature* 456:967–970.
26. Riobo NA, Saucy B, Dilizio C, Manning DR (2006) Activation of heterotrimeric G proteins by Smoothened. *Proc Natl Acad Sci USA* 103:12607–12612.
27. DeCamp DL, Thompson TM, de Sauvage FJ, Lerner MR (2000) Smoothened activates Galphai-mediated signaling in frog melanophores. *J Biol Chem* 275:26322–26327.
28. Hammerschmidt M, McMahon AP (1998) The effect of pertussis toxin on zebrafish development: A possible role for inhibitory G-proteins in hedgehog signaling. *Dev Biol* 194:166–171.
29. Low WC, et al. (2008) The decoupling of Smoothened from Galphai proteins has little effect on Gli3 protein processing and Hedgehog-regulated chick neural tube patterning. *Dev Biol* 321:188–196.
30. Hengl T, et al. (2010) Molecular components of signal amplification in olfactory sensory cilia. *Proc Natl Acad Sci USA* 107:6052–6057.
31. Whitfield JF (2008) The solitary (primary) cilium—a mechanosensory toggle switch in bone and cartilage cells. *Cell Signal* 20:1019–1024.
32. Gu X, Olson EC, Spitzer NC (1994) Spontaneous neuronal calcium spikes and waves during early differentiation. *J Neurosci* 14:6325–6335.
33. Zhang J, Rosenthal A, de Sauvage FJ, Shivdasani RA (2001) Downregulation of Hedgehog signaling is required for organogenesis of the small intestine in Xenopus. *Dev Biol* 229:188–202.
34. Holliday J, Adams RJ, Sejnowski TJ, Spitzer NC (1991) Calcium-induced release of calcium regulates differentiation of cultured spinal neurons. *Neuron* 7:787–796.
35. Orellana SA, McKnight GS (1992) Mutations in the catalytic subunit of cAMP-dependent protein kinase result in unregulated biological activity. *Proc Natl Acad Sci USA* 89:4726–4730.
36. Rogers KV, Goldman PS, Frizzell RA, McKnight GS (1990) Regulation of Cl- transport in T84 cell clones expressing a mutant regulatory subunit of cAMP-dependent protein kinase. *Proc Natl Acad Sci USA* 87:8975–8979.
37. Boulay G, et al. (1999) Modulation of Ca(2+) entry by polypeptides of the inositol 1,4, 5-trisphosphate receptor (IP3R) that bind transient receptor potential (TRP): Evidence for roles of TRP and IP3R in store depletion-activated Ca(2+) entry. *Proc Natl Acad Sci USA* 96:14955–14960.
38. Bobanovic LK, et al. (1999) Molecular cloning and immunolocalization of a novel vertebrate trp homologue from Xenopus. *Biochem J* 340:593–599.
39. Shim S, et al. (2005) XTRPC1-dependent chemotropic guidance of neuronal growth cones. *Nat Neurosci* 8:730–735.
40. Wang GX, Poo MM (2005) Requirement of TRPC channels in netrin-1-induced chemotropic turning of nerve growth cones. *Nature* 434:898–904.
41. Suh BC, Inoue T, Meyer T, Hille B (2006) Rapid chemically induced changes of PtdIns (4,5)P2 gate KCNQ ion channels. *Science* 314:1454–1457.
42. Briscoe J, Pierani A, Jessell TM, Ericson J (2000) A homeodomain protein code specifies progenitor cell identity and neuronal fate in the ventral neural tube. *Cell* 101: 435–445.
43. Tertyshnikova S, Fein A (1998) Inhibition of inositol 1,4,5-trisphosphate-induced Ca2+ release by cAMP-dependent protein kinase in a living cell. *Proc Natl Acad Sci USA* 95: 1613–1617.
44. Ben-Ari Y, Spitzer NC (2010) Phenotypic checkpoints regulate neuronal development. *Trends Neurosci* 33:485–492.
45. Pineda RH, Ribera AB (2008) Dorsal-ventral gradient for neuronal plasticity in the embryonic spinal cord. *J Neurosci* 28:3824–3834.
46. McLean DL, Fan J, Higashijima S, Hale ME, Fetcho JR (2007) A topographic map of recruitment in spinal cord. *Nature* 446:71–75.
47. McLean DL, Fetcho JR (2009) Spinal interneurons differentiate sequentially from those driving the fastest swimming movements in larval zebrafish to those driving the slowest ones. *J Neurosci* 29:13566–13577.
48. Provine RR, Sharma SC, Sandel TT, Hamburger V (1970) Electrical activity in the spinal cord of the chick embryo, in situ. *Proc Natl Acad Sci USA* 65:508–515.
49. Breunig JJ, et al. (2008) Primary cilia regulate hippocampal neurogenesis by mediating sonic hedgehog signaling. *Proc Natl Acad Sci USA* 105:13127–13132.
50. Han YG, et al. (2008) Hedgehog signaling and primary cilia are required for the formation of adult neural stem cells. *Nat Neurosci* 11:277–284.
51. Heo JS, Lee MY, Han HJ (2007) Sonic hedgehog stimulates mouse embryonic stem cell proliferation by cooperation of Ca2+/protein kinase C and epidermal growth factor receptor as well as Gli1 activation. *Stem Cells* 25:3069–3080.
52. Osawa H, et al. (2006) Sonic hedgehog stimulates the proliferation of rat gastric mucosal cells through ERK activation by elevating intracellular calcium concentration. *Biochem Biophys Res Commun* 344:680–687.